2-6-2018

Nonthermal ice nucleation observed at distorted contact lines of supercooled water drops

Fan Yang
Michigan Technological University

Owen Cruikshank
Michigan Technological University

Weilue He
Michigan Technological University

Alexander Kostinski
Michigan Technological University

Raymond Shaw
Michigan Technological University

Nonthermal ice nucleation observed at distorted contact lines of supercooled water drops

Fan Yang,[1,*] Owen Cruikshank,[2] Weilue He,[3] Alex Kostinski,[1] and Raymond A. Shaw[1,†]
[1]*Department of Physics, Michigan Technological University, Houghton, Michigan 49931, USA and Atmospheric Sciences Program, Michigan Technological University, Houghton, Michigan 49931, USA*
[2]*Department of Physics, Michigan Technological University, Houghton, Michigan 49931, USA*
[3]*Department of Biomedical Engineering, Michigan Technological University, Houghton, Michigan 49931, USA*

(Received 19 September 2017; revised manuscript received 20 December 2017; published 6 February 2018)

Ice nucleation is the crucial step for ice formation in atmospheric clouds and therefore underlies climatologically relevant precipitation and radiative properties. Progress has been made in understanding the roles of temperature, supersaturation, and material properties, but an explanation for the efficient ice nucleation occurring when a particle contacts a supercooled water drop has been elusive for over half a century. Here, we explore ice nucleation initiated at constant temperature and observe that mechanical agitation induces freezing of supercooled water drops at distorted contact lines. Results show that symmetric motion of supercooled water on a vertically oscillating substrate does not freeze, no matter how we agitate it. However, when the moving contact line is distorted with the help of trace amounts of oil or inhomogeneous pinning on the substrate, freezing can occur at temperatures much higher than in a static droplet, equivalent to $\sim 10^{10}$ increase in nucleation rate. Several possible mechanisms are proposed to explain the observations. One plausible explanation among them, decreased pressure due to interface curvature, is explored theoretically and compared with the observational results quasiquantitatively. Indeed, the observed freezing-temperature increase scales with contact line speed in a manner consistent with the pressure hypothesis. Whatever the mechanism, the experiments demonstrate a strong preference for ice nucleation at three-phase contact lines compared to the two-phase interface, and they also show that movement and distortion of the contact line are necessary contributions to stimulating the nucleation process.

DOI: 10.1103/PhysRevE.97.023103

I. INTRODUCTION

Conditions under which supercooled water freezes are not only crucial for determining the precipitation efficiency of clouds and the vertical profile of water within the Earth's atmosphere, but also underlie fields as diverse as evolution in extreme environments, food preservation, and the design of anti-icing surfaces [1–7]. Most work has focused on the roles of temperature, supersaturation, and ice-nucleating material properties [8,9]. Indeed, temperature is nearly universal in its use within the atmospheric ice nucleation community: ice nucleation rate depends exponentially on temperature [10], ice supersaturation is a function of temperature, ice-nucleating materials are characterized by their freezing temperatures, and finally, even the name: supercooled water. In contrast, the experiments reported here are about stretched or distorted water under isothermal conditions. While it has long been noted that supercooled water can freeze instantly by shaking or tapping [11], little attention has been devoted to nonthermal, mechanical effects.

The simple thought that guides us is that, because of the water density anomaly it is easier for supercooled water to freeze at lower densities, and therefore lower pressures. There is some experimental evidence in the opposite direction of this argument: Kanno *et al.* [12] reported supercooling of 70 K at pressures of 2100 atmospheres, compared to 38 K at 1 atmosphere. Our heuristic perspective is that what can be accomplished by thermal means (δT), can also be achieved by mechanical ones (δp). Indeed, molecular dynamics simulations show that low density is strongly related to ice crystallization [13,14]. To that end, here we devise experiments to subject supercooled water drops to mechanical agitation and tensile stresses, under isothermal conditions; thus, the adjective "nonthermal" in the title.

The motivating, long-standing mystery is the observation that supercooled water droplets freeze at a higher temperature when an ice-nucleating particle impacts the water surface (contact nucleation), compared to the same particle being immersed in the droplet (immersion nucleation) [2,15]. Several possible mechanisms have been proposed, including existence of ice embryos on impacting particles, reduction of the free-energy barrier for ice nucleation through impaction, role of the three-phase contact line and propagation of pressure waves, but the evidence is sparse and inconclusive [16–20]. Recent experiments show that the phenomenon is more universal than previously thought: rather than suppressing the melting point, soluble salts nucleate ice on contact with supercooled water [21], and an external contact crystallizes salt in a supersaturated solution droplet [22]. Although the underlying mechanism remains a mystery, empirical representation in cloud models show that contact nucleation is as important as immersion nucleation for ice production in the atmosphere [23]. Therefore, it is crucial to understand contact nucleation to fully explore the role of ice nucleation for clouds, weather and climate.

*Currently at Brookhaven National Laboratory.
†rashaw@mtu.edu

Our experiments explore the possible role of mechanical agitation, and the resulting motion of the three-phase contact line, as a trigger of ice nucleation. We observe a single water drop resting on a substrate subjected to vertical oscillations at a constant temperature significantly higher than the natural freezing temperature of the substrate. The location of freezing of the supercooled drop is pinpointed using high-speed imagery, as in earlier work [24,25] but emphasizing dynamic effects. Traces of oil and substrates with inhomogeneous pinning properties are used to further distort the contact lines. The question is, will the stretched or disturbed contact lines cause water to freeze at anomalously high rates?

II. EXPERIMENTAL APPROACH

Toward the goal of understanding the physical origin of contact nucleation, here we study heterogeneous liquid-to-ice nucleation with a uniform, smooth substrate functioning as the nucleating agent. The experiments are carried out under isothermal conditions to avoid thermal gradients. In earlier work we focused on the spatial preference for nucleation at the substrate-water-air contact line [20,24–26]. We continue with that approach, with a clean, well defined contact line resulting from the simple sessile drop geometry, but here we introduce contact line motion through substrate oscillation. The spatial distribution of nucleation sites is monitored via high-speed imaging of droplet freezing with an overhead camera. We begin by determining the inherent (natural) freezing temperature of the substrate for a still droplet of a given size (30 μl). The moving-contact-line experiments are then conducted at temperatures well above the natural freezing temperature, such that the probability of freezing for a still droplet is not observable.

Experiments were carried out inside an insulated, isothermal container (Engel MHD13F-DM), with controllable temperature down to -18^{o} C. The original top cover is replaced by a self-made lid with a small optical window at the center. A high-speed camera (Photron SA6) is mounted above the optical window, and a round LED light is attached below the top lid to illuminate the droplet. A speaker (Tang Band W3-2108) sits inside of the freezer just below the optical window. The speaker is driven by a function generator (Frederiksen), and the frequency and amplitude of the speaker are calibrated by a laser vibrometer.

A 0.22-mm-thick glass substrate is attached to the top of the speaker. Substrates were washed with acetone, alcohol, and distilled water, and dried with a clean, filtered, low-humidity air flow before the experiment. A flow of filtered dry air (2 L min^{-1}) is fed into the freezer to decrease the inside relative humidity and to ensure no dew or frost can form on the substrate at temperatures above $-20\,^{\circ}$C. After three hours the freezer is in a steady state, and the temperature is $-17.0 \pm 0.5\,^{\circ}$C, which is measured by a RTD probe near the substrate. Two types of substrates are used in the study: silica glass (Hampton Research Corp., HR8-082) and polydimethylsiloxane (PDMS). The preparation of the PDMS substrate is detailed in the Appendix.

For the freezing experiments described in this work, a 30 μl droplet of type 1 grade water (distilled, deionized, UV-irradiated) is set at the center of the substrate motionlessly for 10 minutes before the speaker is turned on, to make sure droplet reaches the equilibrium temperature. The characteristic thermal diffusion time for droplet is about 1 min (estimated via $\tau \approx V^{2/3}/\alpha$, where α is the thermal diffusivity of water [26]). A RTD probe near the droplet also confirms that the temperature reaches a steady state well within the 10 minutes. The speaker is then turned on with a specified frequency and amplitude. The oscillating drop is observed for 10 s and occurrence (or absence) of freezing is recorded. An inclined mirror is placed at the edge of the speaker, and the overhead camera can also be used to record a side view when needed.

III. RESULTS

A. Droplet motion on a vertically oscillating substrate

The response of sessile droplets on a vertically oscillating plane has been well studied [27,28]. The resonant frequency of the sessile droplet mainly depends on the mass of the droplet and the contact angle. To find the resonant frequency, we record the response of the droplet from a side view by increasing the frequency in 5 Hz increments, at a small amplitude. The resonant frequency for the first mode of a 30 μl droplet on the silica glass substrate is approximately 55 Hz. For the vibrational freezing experiment, we use 30 Hz, because we want to be away from the resonant frequency to keep the motion of the droplet simple.

A sessile droplet on a constant-frequency, vertically oscillating substrate experiences two types of oscillations [27]: (1) at small amplitude, the contact line remains pinned, resulting in contact angle hysteresis; (2) at large amplitude, the contact line can move. The relative spreading distance of a 30 μl pure water droplet on a silica glass substrate, for various amplitudes at a vibration frequency of 30 Hz are shown in Fig. 1(a). Here we use the maximum speed of the substrate $v_{\max}$ to represent the amplitude. The amplitude is as small as 0.36 mm for $v_{\max} = 6.7$ cm/s, and as large as 3.7 mm for $v_{\max} = 69.0$ cm/s. The contact line does not move when $v_{\max} < 28.6$ cm/s due to pinning on the substrate. The results also show that relative spreading of the drop is repeated within one oscillation cycle between 28.6 cm/s and 42.2 cm/s, while it is repeated within two vibrational cycles between 49.1 cm/s and 69.0 cm/s. This nonsymmetric behavior at higher amplitude is because one satellite droplet becomes separated from the parent droplet vertically every other oscillation cycle. The smallest spreading distance is where the detachment occurs. The detached satellite droplet can merge with the parent droplet, and a new cycle starts (see Appendix). When $v_{\max} > 69.0$ cm/s, the droplet will quickly either shift off of the substrate, or breakup to several small satellite droplets within 10 seconds, and therefore is not considered in this study.

B. Freezing on a vertically oscillating substrate

The freezing fractions of a 30 μl drop of pure water on vertical oscillating silica glass substrate for different amplitudes at 30 Hz are shown in Fig. 1(a). Experiments are repeated ten times for each case. As shown by the red bars, ice nucleation is not triggered on the silica glass substrate over the full range of amplitude. Apparently, although the existence of a moving contact line was observed to be necessary in prior experiments

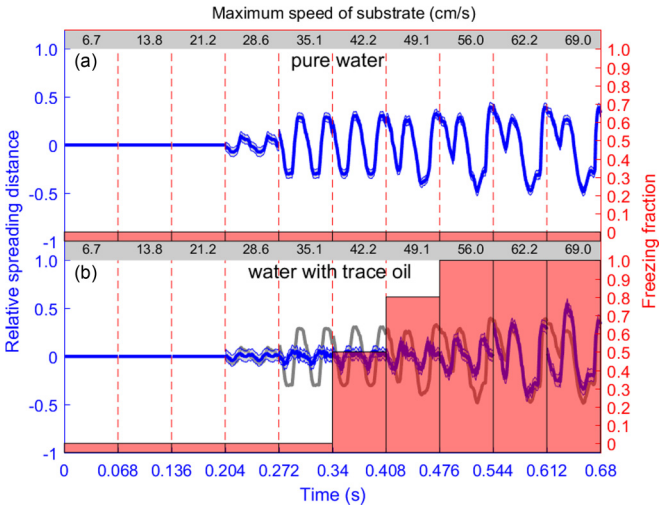

FIG. 1. Response of a 30 μl (a) pure water and (b) water with a trace amount (10 mg/ml) of pump oil on a silica glass substrate for different amplitudes at 30 Hz and $-17.0 \pm 0.5\,^{\circ}$C. Amplitude is represented by the maximum velocity (v in unit of cm/s) of the substrate for each case, with $v = \omega A$. Equal-time increments from individual experiments are separated by vertical red dash lines. The thick blue line is the relative spreading distance measured from a side view. The thin blue line is the estimated uncertainty. The relative spreading distance is defined as $[D(t) - D_0]/D_0$, where $D(t)$ is the diameter captured from the side view using 1000 Hz frame rate with 27.8 μm resolution, and D_0 is the diameter of droplet before vibration. Gray lines in (b) are the response of pure water for comparison. The red bars represent the fraction of drops that experience freezing (freezing probability) for each case.

[25], it is not sufficient for initiating nucleation of ice in supercooled water.

To introduce contact-line distortions, we added just a trace amount of oil to the water droplet, anticipating that isolated pockets of oil form along the contact line [29]. The preparation of the oil-water mixture is detailed in the Appendix. Indeed, despite only the trace amount of oil, the results change dramatically. Figure 1(b) shows that the contact line de-pins without ice nucleation at low amplitude ($v = 28.6$ and 35.1 cm/s) similar to pure water. However, the oil-spiked droplet freezes at higher amplitude, in contrast with the pure-water oscillating droplet that never freezes. The freezing probability is observed to increase with oscillation amplitude. The relative spreading distance for the oil-spiked drop is much smaller than that for the pure water drop at small amplitude (between 28.6 and 56.0 cm/s). This may result from the large viscosity of the traces of oil around the drops. At larger amplitude (62.2 and 69.0 cm/s), the relative spreading distances of water with trace amount of oil are similar to or even larger than that of pure water. It might be due to the bias of the relative spreading distance calculation based on the side view camera, compared to the quite asymmetric spreading distance for water with trace amount of oil viewed from the top.

Selected time-resolved images of drop oscillation and onset of freezing (Fig. 2 and in Supplemental Material Movies S1 and S2 [30]) show that while the pure water drop does not freeze at all, the oil-spiked drop always freezes, and does so at the contact line. For pure water, the drop oscillates with a de-pinned contact line but no freezing occurs. For the water with a trace of oil, the droplet oscillates before freezing, but the maximum spreading area is smaller than for pure water. Inspection of the freezing onset shows that it always starts from the drop edge, near the contact line, and that sometimes it can even start from multiple points around the edge, as shown in Fig. 2(B4). This phenomenon is reminiscent of the electrowetting experiment: freezing from the edge and from multiple points [25]. We therefore anticipate that the mechanism of ice nucleation in the two cases should be similar.

C. Locally curved contact line

The starkly different freezing behavior of the water with a trace of oil compared with pure water seems to be related to the different contact-line response during oscillation. The high-speed camera images show that the shape of the pure water drop remains symmetric (spherical-cap shape) during the oscillations (see Fig. 2(A) and more clearly in Supplemental Material Movie S1 [30]), whereas the shape of the water-oil droplet does not (see Fig. 2(B) and more clearly in Supplemental Material Movie S2 [30]). Instead, the contact line often becomes strongly distorted from its static, circular shape, and one example of the distortion is shown in Fig. 3(a) and Supplemental Material Movie S3 [30]. The contact line distortion during oscillation is likely a result of nonuniform distribution of oil at the surface due to the Plateau-Rayleigh instability [31]. Previous observations do show that oil is not uniformly distributed around the droplet [29], and our measurements confirm that after complete evaporation of the water drop, a ring of small oil droplets remains behind (see the Appendix). The portions of the contact line containing viscous oil will move slower than the rest, with differential velocity leading to local distortions of the contact line. It should be mentioned that we cannot see whether there are pockets of oil along the contact line or there are some tiny oil droplets inside the droplet, because the oil concentration is very low. However, we do clearly observe that the response of the drop on the vertically oscillating substrate is quite different when we add such a trace amount of oil. Why such a small amount of oil changes the response and behavior of the oscillating droplet is an interesting question by itself and merits further investigation.

Is it the distortion of the contact line or the oil that triggers freezing? To disentangle the two, we use an oil-free water drop on a silica glass substrate with a thin spin-coated PDMS layer. This substrate has physical (e.g., irregularities in surface morphology) or chemical (e.g., stains or inhomogeneities) defects on a surface that lead to strong pinning of the contact line [31]. As discussed already (Fig. 1), pinning also exists on the silica glass substrate, as manifested by the contact angle hysteresis. But that pinning on silica glass is quite uniform and homogeneous and does not distort the spherical shape of the droplet during oscillation. In contrast, as shown next, inhomogeneous, localized pinning on the PDMS substrate generates a curved contact line and triggers nucleation.

The high-speed camera confirms that the shape of a pure water droplet on a PDMS substrate, during oscillation with contact line motion, is not symmetric due to locally strong

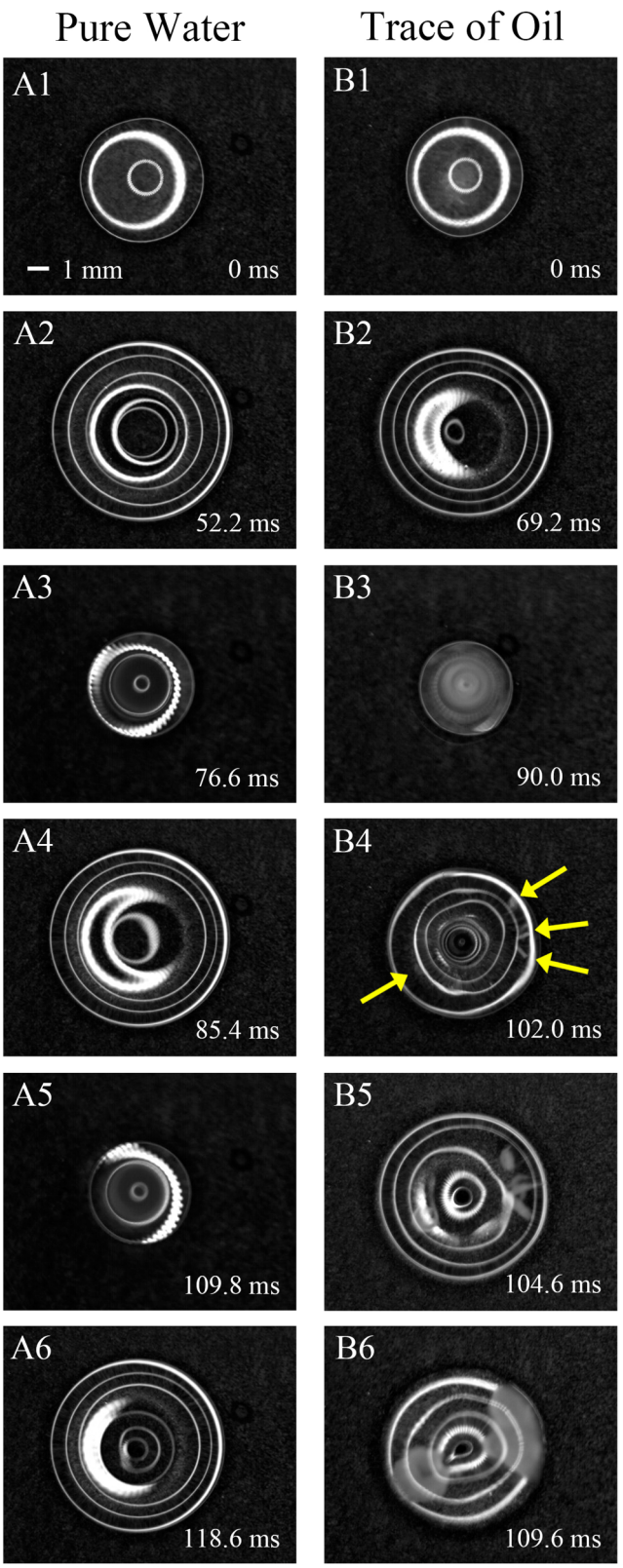

FIG. 2. Individual video frames, taken with the high-speed camera (5000 fps), showing pure water (**left**) and water with a trace (10 mg/ml) of pump oil (**right**) at different stages of oscillation on a silica glass substrate with 30 Hz and $v_{max} = 56.0$ cm/s (see Supplemental Material Movie S1 for pure water [30] and Supplemental Material Movie S2 for water with a trace of oil [30]). (A1) and (B1) represent the state before oscillation. For water, (A2), (A4), and (A6) are examples of maximum spreading area, while (A3) and (A5) are examples of minimum spreading area. For the water with a trace of oil, (B2) is an example of maximum spreading area and (B3) is an example of minimum spreading area before freezing. (B4), (B5), and (B6) show how ice nucleates at the edge and how it propagates inward. Yellow arrows point out the multiple ice nucleation sites.

pinning (see Fig. 3(b) and Supplemental Material Movie S4 [30]). Consistently, the contact line movement is also suppressed on the PDMS substrate compared with the silica glass substrate [Fig. 4(a)]. This is also consistent with the observed contact angle hysteresis: the advancing and receding contact angles on PDMS are $114 \pm 5.4\,^{\circ}$C and $90 \pm 5.4\,^{\circ}$C, respectively, with the difference larger than that for the silica glass substrate. The natural freezing temperature for a static water drop on PDMS is $-24.2 \pm 0.4\,^{\circ}$C. However, oscillating drops on PDMS at $-17\,^{\circ}$C are observed to freeze only after the contact line begins to move [Fig. 4(b)], and again, the nucleation sites are all near the contact line. Water on strongly-pinning PDMS therefore behaves analogously to water with a trace of oil on silica glass, which brings us back to the distorted contact line as a trigger for ice nucleation. Experiments are also done at two higher temperatures, $-11\,^{\circ}$C and $-14\,^{\circ}$C, for pure water drop on PDMS substrates to investigate the combined effect of temperature and vibration on ice nucleation. Results in Fig. 4(b) show that the freezing probability at a higher temperature is nearly compensated by more intense agitation (higher oscillation amplitude). For example, a freezing probability near 0.5 is observed for $-17\,^{\circ}$C when there is a relatively low amplitude of 49.1 cm/s; then for $-14\,^{\circ}$C requires 56.0 cm/s, and finally at $-11\,^{\circ}$C a relatively high amplitude of 62.2 cm/s is required.

IV. DISCUSSION

A. Various ice nucleation causes ruled out

The observed differences in freezing behavior cannot be attributed to temperature because the experiments are isothermal and drops are held well above the static freezing temperature. Indeed, the oscillating drop experiments are performed at a constant temperature of $-17.0\,^{\circ}$C (with $0.5\,^{\circ}$C uncertainty), much higher than the natural freezing temperature of oil-spiked water on a silica glass substrate (around $-25.8\,^{\circ}$C). Note that the difference of 8.6 K is huge in the nucleation theory context: the ice nucleation rate at $-17.0\,^{\circ}$C is about 10 orders of magnitude smaller than that at $-25.6\,^{\circ}$C [10]. In fact, a static droplet survives as a supercooled liquid for several hours on the substrate until it completely evaporates. The natural freezing temperature of $-25.8\,^{\circ}$C was determined using the approach described in prior work [24,26]. Briefly, the substrate is set on a cold stage with a 2 K/min cooling rate, and the stage temperature is recorded when the droplet freezes "naturally," i.e., without any external agitation.

Furthermore, onset of freezing in the oil-spiked drops cannot be attributed to oil-induced changes in freezing temperature. The natural freezing temperatures for a static water drop with a 10 mg/mL trace of oil on a silica glass substrate is

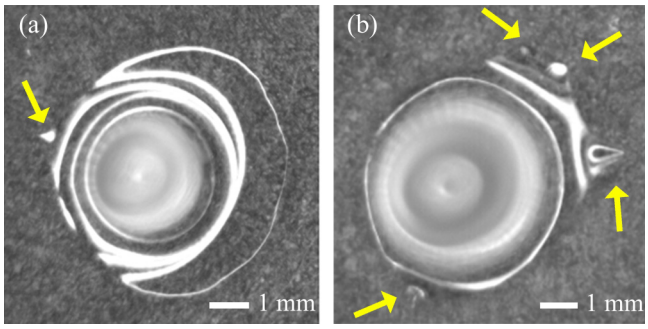

FIG. 3. Example of macroscopic pinning behavior during oscillation of (a) the water droplet with a trace of oil, on a silica glass substrate (see Supplemental Material Movie S3 [30]) and (b) pure water on a PDMS substrate (see Supplemental Material Movie S4 [30]). Yellow arrows indicate the locally curved contact line.

$25.8 \pm 0.6\,^{\circ}\mathrm{C}$, equal to that for a pure water droplet, $25.6 \pm 0.6\,^{\circ}\mathrm{C}$. No suppression of freezing temperature occurs, as the solubility of pump oil in water is less than 10^{-2} mg/ml (determined by the observed separation of oil and water at that concentration). This is in contrast to some other reports that ice nucleation can be initiated by hydrocarbons at static contact lines [32].

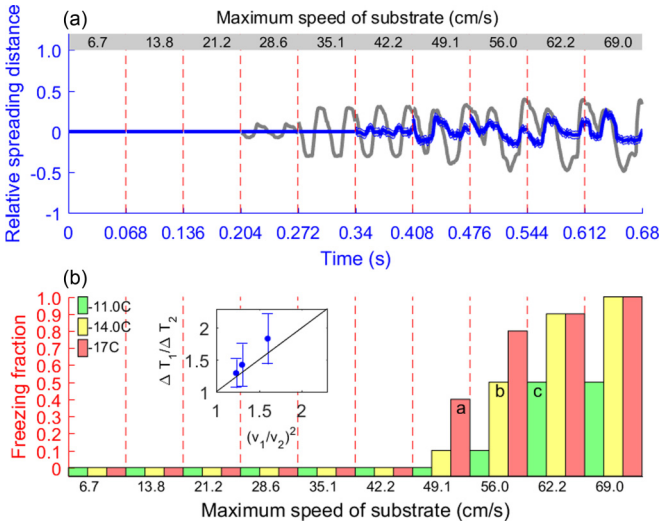

FIG. 4. (a) Response of a 30 μl pure water droplet on a PDMS substrate for different amplitudes at 30 Hz. Format and line styles are as in Fig. 1. The contact line starts to move when $v_{\max} \geqslant 42.2$ cm/s, substantially larger than that observed for the silica glass substrate. (b) Fraction of droplets that freeze for different amplitudes with 30 Hz at three temperatures. The green, yellow, and red bars represent the freezing fraction for each case at $-11.0 \pm 0.5\,^{\circ}\mathrm{C}$, $-14.0 \pm 0.5\,^{\circ}\mathrm{C}$, and $-17.0 \pm 0.5\,^{\circ}\mathrm{C}$, respectively. The natural freezing temperature for a static water drop on PDMS is $-24.2 \pm 0.4\,^{\circ}\mathrm{C}$. The inset shows the ΔT vs. Δp scaling discussed in the text, with $\Delta p_c/\Delta p_b \sim (v_c/v_b)^2 \sim (62.2/56.0)^2 = 1.23$ compared to $\Delta T_c/\Delta T_b = (24.2 - 11.0)/(24.2 - 14.0) = 1.29$, $\Delta p_b/\Delta p_a \sim 1.30$ compared to $\Delta T_b/\Delta T_a = 1.42$, and $\Delta p_c/\Delta p_a \sim 1.60$ compared to $\Delta T_c/\Delta T_a = 1.83$ (a, b, and c are labeled in the red, yellow, and green bars, respectively, with near 0.5 freezing probability). Note that $\Delta T_1/\Delta T_2$ is closer to $(v_1/v_2)^2$, as opposed to v_1/v_2 or $(v_1/v_2)^3$. Uncertainties shown represent the observed temperature variability.

Could the trace amount of oil change the contact angle, and thereby render it a more efficient nucleator? This is not so, because the contact angle of water with a 10 mg/ml trace of oil on the silica glass substrate is $99 \pm 2.7\,^{\circ}\mathrm{C}$, only slightly larger than for pure water ($94\,^{\circ}\mathrm{C}$). The difference between advancing and receding contact angles is a measure of the pinning on silica glass substrates [31], and this contact angle hysteresis also does not change. The receding and advancing contact angles for the oil-spiked water are $79 \pm 4.0\,^{\circ}\mathrm{C}$ and $101 \pm 2.5\,^{\circ}\mathrm{C}$, respectively, similar to pure water $79 \pm 3.9\,^{\circ}\mathrm{C}$ and $101 \pm 7.7\,^{\circ}\mathrm{C}$. This similarity is consistent with the fact that the contact line of the pure water and of the oil-spiked water are both depinned for $v_{\max} \geqslant 28.6$ cm/s. Further investigations on the influence of oil concentration and type on the freezing behavior are provided in the Appendix. In summary, chemical or surfactant properties of oil cannot account for the observed freezing.

The observation that freezing always starts from the droplet edge may suggest evaporative-cooling at the edge and possible Marangoni flow. However, evaporation-induced freezing is unlikely in our experiments for several reasons. Because the droplet is set on a temperature controlled substrate, the temperature is highly uniform [26]. Furthermore, if evaporative cooling plays a role, we should find that ice nucleation is preferred at the contact line even in static droplets, but previous experiments show that the ice nucleation sites in such drops are Poisson distributed [24]. In addition, the evaporation rate also depends on the humidity of the environmental air. However, we did not observe any indication that the droplet freezing temperature changes with relative humidity in our experiment.

A possible role of frost or other surface defects is also ruled out because a pure water drop experiences no freezing on the same substrate, and because no freezing occurs in the oil-spiked water drop at small oscillation amplitude even when the contact line is moving back and forth. An explanation depending on a special ice-nucleating surface site is also difficult to reconcile with the observation of freezing simultaneously initiated at multiple points. Usually, nucleation by a point defect is followed by nearly instant freezing of the full drop [24].

B. Possible ice nucleation mechanisms

Anything related to the static droplet cannot be the reason for freezing observed in our experiments. Furthermore, any mechanism simply related to agitation of water cannot account for the observed universal occurrence of ice nucleation at the three-phase contact line. Whatever the mechanism, it must be related to drop oscillation and the existence of a moving contact line. However, vibration is a necessary but not sufficient condition for freezing, because for pure water on the silica substrate, we cannot trigger ice nucleation no matter how we agitate the droplet. High-speed camera images, although not providing proof at the current stage, strongly suggest that distortion of the contact line, generated through either trace amounts of oil or substrates with inhomogeneous pinning, is related to the freezing observed in our experiments. In this subsection, we will discuss possible ice nucleation mechanisms worth investigating in the future.

All of the observations thus far are compatible with the distortion or strong curvature of a moving contact line as a cause. The detailed structure and processes occurring during

stretching or nonuniform motion of a a three-phase contact line may be highly complex. We therefore begin our search for an explanation with the simplest working hypothesis. How can a curved contact line be connected to ice nucleation, a process notable for its strong temperature dependence?

One possible mechanism is that distorted contact line might reinforce the evaporation rate a the edge, and thus trigger ice nucleation due to enhanced evaporative cooling. Although we cannot quantify the local evaporation rate in our experiments, what we know is that evaporative cooling has little effect on static drops or symmetrically oscillating drops in our experiments. More research is necessary to investigate whether deformation of drops can enhance the evaporation rate locally, and if true, whether such enhanced evaporation would be enough to explain the observed increasing freezing temperature here.

Fundamentally, the enhanced evaporation hypothesis relies on temperature. Instead of temperature, pressure perturbations due to the distorted contact line might be another possible mechanism for freezing observed in our experiments. Indeed, the degree of metastability is almost universally characterized by the degree of supercooling δT, especially in the atmospheric science community. However, it can also be characterized by δp, the pressure difference between the metastable and the equilibrium phases. In fact, the two variables are related in a Clausius-Clapeyron-like fashion, $\delta p = (l_f/T_0\Delta v)\delta T$, where l_f is the latent heat of fusion and Δv is specific volume difference of water and ice (see section 162 and page 535 of Landau and Lifshitz [33]; we note in passing that δp and δT are metastable changes are therefore not along the coexistence curve, and l_f is not the equilibrium value [34]).

Distortion of the contact line might generate Laplace pressure perturbations or shear stresses, which in turn can affect ice nucleation in several ways. First, strong negative pressure perturbations can lead to cavity formation and collapse, which benefit ice nucleation [35–40]. Second, pressure perturbations might change the water-ice interfacial free energy, and thus influence the ice nucleation rate [41]. In addition, pressure perturbations can directly change the chemical potential between ice and supercooled water, and thus affect the energy barrier of the phase change [42,43].

C. Pressure perturbation hypothesis

All the possible mechanisms discussed above are physically reasonable, and we cannot confirm which is valid at the current stage based on our experiments. More experimental, computational, and theoretical work is needed to understand the details of the ice nucleation process in the experiments we have described. Among all the possible mechanisms, changing of chemical potential due to pressure perturbation is explored here in more depth because of supporting theoretical findings Li *et al.* [42] and the ability to compare results with at least semi-quantitative theoretical expectations.

Recent work shows that such a pressure perturbation (Δp) affects the chemical potential difference ($\Delta\mu$) between ice and water as [42,43]

$$\Delta\mu = l_f \frac{\Delta T}{T_0} + \Delta p \Delta v, \tag{1}$$

where $\Delta v = v_l - v_s$. Δp can be either a positive or negative pressure perturbation. Because Δv is negative for the water-ice system (i.e., water density anomaly), the sign of Δp determines whether pressure will increase or decrease the driving force for a phase change $\Delta\mu$, thus enhancing or suppressing the ice nucleation rate J. For example, the Laplace pressure of a nanodroplet is positive and may explain why nanoscale supercooled droplets can survive at very low temperature without phase change [42]. Conversely, it has also been observed that deeply negative pressure in a liquid capillary bridge allows ice to form at high temperatures [44].

We address this semiquantitatively by asking, what is the negative pressure perturbation needed to compensate the diminishing effect of high temperature on ice the nucleation rate? Based on classical nucleation theory and Eq. (1), such pressure perturbation is proportional to the temperature difference and can be expressed as (detailed derivation is given in the Appendix),

$$\Delta p = \frac{l_f}{T_0 \Delta v} \Delta T. \tag{2}$$

Thus, to balance the suppression of ice nucleation rate resulting from a $\sim$1 K temperature increase, a negative pressure of $\sim 10^7$ Pa is required. To illustrate the plausibility of Eq. (2), we note the consistency with measurements of Kanno *et al.* [12]: water supercooling of $\delta T = 38$ K at 1 atmosphere versus $\delta T = 70$ K at 2100 atmospheres. It implies $\Delta T = 32$ K and $\Delta p = 2099$ atmospheres, whereas a rough estimate using Eq. (2) yields $\Delta p = 3200$ atmospheres for the same ΔT.

The notion of pressure-induced nucleation may be broadened to imply that ice formation is favored when water is either supercooled or stretched. Can the compensation between temperature and negative pressure (or other off-diagonal terms of the stress tensor [34,45]) be tested experimentally? To that end, the inset in Fig. 4(b) shows that the freezing probability can be approximately maintained even at a higher temperature, if compensated by higher oscillation amplitude. To test the compensation condition quantitatively, we note that Eq. (2) yields $(\Delta T)_1/(\Delta T)_2 = (\Delta p)_1/(\Delta p)_2$, where 1 and 2 denote the experimental conditions at different (p,T) but with the same ice nucleation rate. Guided by the general thermodynamic perspective on pressure as energy volume density, $p = \partial U/\partial V \sim U/V$, and associating Bernoulli-type scaling $\sim\rho v^2$ with Δp, we see in the inset of Fig. 4(b) that the equality is supported to within the experimental uncertainty.

One related question is that whether such high negative pressure perturbation is achievable in water. It is known that vapor nucleation occurs in water at a maximum negative pressure around -3×10^7 Pa [46]. Larger negative pressure perturbation can be generated through submicron cavity collapse [35,36,40]. Although we have no direct evidence supporting it, it is plausible that the moving, distorted contact lines lead to cavity formation through relatively small pressure perturbations. The collapse of the cavity then produce very high positive, and then negative pressure, which can lower the freezing temperature of supercooled water [37–39]. Regardless of the details, and still lacking direct evidence, the observations of enhanced freezing are at least consistent with a role of negative pressure and therefore can motivate further work. Recalling that a $\sim$1 K temperature increase is compensated

by a negative pressure of $\sim 10^7$ Pa, the latter corresponding to a radius of curvature on the order of 10 nm assuming static Laplace pressure. Being equilibrium estimates, these values are likely overly stringent because gradients are present. Nevertheless, even these values are plausibly achieved, given observations of surface roughness, pinning deformation, and cavity collapse [36,47–49].

V. CONCLUDING REMARKS

The oscillating drop experiments described here provide three new observations related to ice nucleation in supercooled water at temperatures for which static droplets are not observed to freeze. First, we observe a strong preference for ice nucleation to occur at the three-phase contact line, rather than at the two-phase substrate–water interface that is typically observed [24]. To be clear, we are unable to determine whether the ice nucleation events occur precisely at the contact line or just near the contact line (localization is determined to within the optical resolution of the imaging system, which is a factor of $\sim$100 times smaller than the typical drop diameter). The observation of nucleation sites occurring near the contact line is in stark contrast to the observation of sites uniformly distributed over the substrate for static droplets [24,26]. Second, we observe that the spatial localization of freezing to the contact line requires, as a necessary but not sufficient condition, movement of the contact line. Third, when freezing occurs in oscillating drops with depinned, moving contact lines, it is always associated with distortion of the contact line. That distortion has been produced in two ways: by addition of trace amounts of oil and by the use of fabricated substrates with local pining defects. In short, the experiments confirm that nonthermal distortion of a moving contact line strongly enhances the freezing of supercooled water. The notion of contact-line-induced ice nucleation provides compelling context for interpretation of many prior experiments: Droplet freezing triggered by impaction of ice nuclei, salt particles, or another supercooled droplet [17,21,50], as well as salt crystallization triggered by impaction [22,51], may all rely on the perturbation of the contact line through collision. In addition, the enhanced ice nucleation at the contact line on particles or nanotextured surfaces may also be a result of the local curved contact line due to strong inhomogeneous pinning [18,20,49,52]. There is also some analogy to the nucleation of nanodroplet and nanobubbles out of oversatured solutions due to chemical or geometric surface heterogeneities [53]. Finally, the results shed light on prior observations of strong enhancement of ice nucleation during transient electrowetting that helped motivate this work [25]. Revisiting the high-speed videos from that study we see distortion of the moving contact line likely due to Rayleigh charge instability (see the Appendix); the results are therefore consistent with the findings presented here.

Why a moving, distorted contact line can enhance ice nucleation is still unclear. Several possible mechanisms are explored in this study, including enhanced evaporative cooling, cavity formation, and collapse due to pressure perturbation, shear stress, change of water-ice interfacial energy, and change of chemical potential. Furthermore, we theoretically explore one possible mechanism in more depth: change of chemical potential due to pressure perturbation. As tentative support we find that the observed freezing-temperature increase scales with contact line speed in a manner consistent with the pressure hypothesis. Of course, we cannot rule out other possible causes in this study and more experiments and simulations are needed to reveal the secrets of the ice nucleation process along moving contact lines. The observations and implications discussed in this paper set the stage for further investigation of moving and distorted contact lines occurring during collisions between droplets and a substrate or particle, their quantitative enhancement of nucleation rate, and their implications for the phenomenon of contact nucleation.

ACKNOWLEDGMENTS

This work was supported by DOE Office of Science as part of the Atmospheric System Research program through Grant No. DE-SC0011690. A. Kostinski acknowledges support from NSF Grant No. AGS-1639868. We thank Dr. W. Cantrell for helpful discussions and Dr. D. Knopf for pointing out the supersaturation possibility. We thank Dr. A. Barnard for assistance with the laser vibrometer measurements, Yujin Sun and Dr. J. W. Drelich for assisting with surface characterization, and Dr. M. C. Frost for providing polymer substrates.

APPENDIX

1. PDMS substrate preparation

The PDMS surface fabrication is accomplished through spin coating. In brief, room temperature vulcanizing PDMS (Dow Corning RTV-3140) was dissolved in toluene and prepared in a 1:5 (w/v) PDMS solution. Siliconized glass coverslips were coated with PDMS using a two-stage spin coating process (Chemat Scientific KW-4A). In the first stage, the coverslip underwent 1000 rpm for 10 s. At the beginning of Stage 1, 500 μl of PDMS solution was pipetted to the center of the spinning coverslip. Then the spin rate was increased to 6000 rpm for another 40 s in Stage 2 for removing the excessive polymer. After spin coating, the PDMS-coated coverslip was left in a chemical hood at room temperature for further air-drying and curing for 20 h. The thickness of the PDMS layer is about 5 μm. This value is estimated from the total mass applied to onto the coverslip, surface area of the coverslip, and the density of RTV-3140. Advancing and receding contact angles are measured with a KRUSS G10 drop shape analyzer.

2. Response of droplets on vertically oscillating plane

The relative spreading distance of a 30 μl pure water droplet on a silica glass substrate, for various amplitudes at a vibration frequency of 30 Hz are shown in Fig. 1(a) (main text). Here we focused on the nonsymmetric behavior of the response of droplets at high amplitude ($v_{\max} \geqslant 49.1$ cm/s). This nonsymmetric behavior is because one satellite droplet becomes separated from the parent droplet vertically every other oscillation cycle. The smallest spreading distance is where the detachment occurs (see Supplemental Material Fig. S1(C) and Movie S5 [30]). The detached satellite droplet can merge with the parent droplet, and a new cycle starts.

When a trace of oil (either pump oil in the main text or mineral oil in the supplement) is added in the water, the contact

angle hysteresis does not change, as shown in Fig. 1(b) and Supplemental Material Fig. S2 [30]; i.e., the contact line of the water with trace oil starts to move when $v_{\max} \geqslant 28.6\,\mathrm{cm/s}$, just as for the pure water. However, the relative spreading distance for the water with trace oil is smaller than that for pure water at the same amplitude and frequency due to the large viscosity of oil.

3. Effect of oil type and oil concentration on ice nucleation through oscillation

To investigate whether the ice nucleation effect observed in the water containing a trace of pump oil is due to unique chemical properties, we also test mineral oil. Results show that there is no significant difference between pump oil and mineral oil (compare Fig. 1(b) and Supplemental Material Fig. S2 [30]). We can also trigger ice nucleation of supercooled water droplets with trace amount of mineral oil through oscillation. High-speed video confirms that ice nucleation always starts near the moving contact line, and can occur at multiple points. One example is shown in Supplemental Material Fig. S3 and Movie S6 [30].

Seven different concentrations (ranging from 10^{-5} to 10 mg/ml) of both pump oil and mineral oil are tested to study the effect of oil concentration on ice nucleation through oscillation. Results show that when the oil concentration is low, the freezing probability is low (see blue lines in Supplemental Material Fig. S4 [30]). The lower limit can be considered an oil concentration of 0, i.e., pure water, for which the freezing fraction is 0. The freezing fraction saturates at probability 1 for high concentrations. However, if we surround the pure water droplet with oil (much higher mixing fraction than 10 mg/ml), then effectively the droplet becomes immobile, and we cannot trigger freezing even at very high amplitude and frequency. So our experiments suggest that to trigger ice nucleation on silica glass substrate upon oscillation, a trace of oil is needed, but too much oil alters the behavior. Results also show that the mean time for onset of freezing after starting the oscillation decreases with increasing oil concentration (see red lines in Fig. S4 [30]). At the highest concentration shown in the figure, the freezing process is sufficiently rapid that it appears by eye to be instantaneous.

4. Oil residue circle on the cover slip

For water with trace oil, a ring of small oil droplets remains on the substrate after the water evaporates completely (see Supplemental Material Fig. S5 [30]). This provides evidence that oil is not uniformly distributed around the droplet.

5. Distorted contact line during electrowetting

In electrowetting experiments (more details in Yang *et al.*, 2015 [25]), the contact line is smooth for a static drop before we turn on the electric field, as shown in Supplemental Material Fig. S6(A) [30]. When the field is switched on, the boundary expends and the contact line become locally curved during this process, as shown in Supplemental Material Fig. S6(B) [30]. The connection between a distorted contact line and electrofreeezing observed in Yang *et al.* (2015) is therefore consistent with the findings of this study [25].

6. Pressure induced ice nucleation rate

Previous computational and theoretical studies show that pressure will affect the chemical potential difference between ice and water for the phase change as [42,43]

$$\Delta\mu = l_f \frac{\Delta T}{T_0} + \Delta p \Delta v, \tag{A1}$$

where $\Delta v = v_l - v_s$. Δp can be either a positive or negative pressure perturbation. Because Δv is negative for the water-ice system (i.e., water density anomaly), the sign of Δp determines whether pressure will increase or decrease the driving force for a phase change $\Delta\mu$, thus enhancing or suppressing the ice nucleation rate J. For example, the Laplace pressure of a nanodroplet is positive and may explain why nanoscale supercooled droplets can survive at very low temperature without phase change [42]. Conversely, it has also been observed that deeply negative pressure in a liquid capillary bridge allows ice to form at high temperatures [44].

Because negative pressure can increase the chemical potential difference between supercooled liquid and ice, we will consider the role of pressure perturbations in the heterogeneous ice nucleation rate. That, in turn, will allow for estimation of the negative pressure required to have the same ice nucleation rate at a higher temperature. The ratio of the heterogeneous ice nucleation rate at a higher temperature T' to that at a lower temperature T at p_0 is [10]

$$\frac{J(p_0,T')}{J(p_0,T)} = \exp\left[-A\left(\frac{T_0^2}{T'\Delta T'^2} - \frac{T_0^2}{T\Delta T^2}\right)\right], \tag{A2}$$

where $A = \frac{16\pi\sigma_{ls}^3 f_{\mathrm{het}}}{3k_B\rho^2 l_f^2}$, k_B is the Boltzmann constant, σ_{ls} is the water-ice surface free energy, ρ is the density of ice, and f_{het} is a geometrical factor accounting for the heterogeneous nucleation efficiency of a substrate. Here we assume the prefactor does not change significantly with temperature. This is roughly true when T' is close to T, compared to the exponential term that is retained. Using Eq. (A1), the ratio of heterogeneous ice nucleation rates is

$$\frac{J(p,T')}{J(p_0,T')} = \exp\left[-\frac{A}{T'}\left(\frac{T_0^2}{(\Delta T' + T_0\Delta p\Delta v/l_f)^2} - \frac{T_0^2}{\Delta T'^2}\right)\right]. \tag{A3}$$

When the enhancement due to pressure perturbation equals the suppression due to temperature, $J(p_0+\Delta p,T') = J(p_0,T)$, which leads to

$$\Delta p\Delta v = \frac{l_f}{T_0}\sqrt{\frac{T}{T'}}\Delta T - \frac{l_f}{T_0}\Delta T'. \tag{A4}$$

If T' is close to T, this can be approximated as

$$\Delta p = \frac{l_f}{T_0\Delta v}(T' - T). \tag{A5}$$

It tells us that the negative pressure needed to have the same ice nucleation rate at a higher temperature is proportional to the temperature difference.

Equation (A1) can also be derived from the perspective of vapor supersaturation just outside the drop at a negatively curved interface. This results in higher rate of deposition ice nucleation. But this is equivalent to the pressure explanation

as we now show. The change in chemical potential for deposition nucleation due to the curvature is $\Delta\mu = RT\ln(\frac{e_{s,r}}{e_{i,r}}) = RT\ln(\frac{e_{s,r}}{e_{s,\mathrm{flat}}}\frac{e_{s,\mathrm{flat}}}{e_{i,\mathrm{flat}}}\frac{e_{i,\mathrm{flat}}}{e_{i,r}})$. Considering the Kelvin effect ($\frac{e_r}{e_{\mathrm{flat}}} = \exp(\frac{2\sigma}{\rho RTr})$), we obtain $\Delta\mu = \frac{2\sigma}{r\rho_l} + l_f\frac{\Delta T}{T_0} - \frac{2\sigma}{r\rho_i} = \Delta v\Delta p + l_f\frac{\Delta T}{T_0}$, which is equivalent to Eq. (A1). The connection makes sense because supersaturation is actually a ratio of pressures. Although the equation is the same, the pressure perturbation mechanism predicts ice nucleation within the liquid phase, while the deposition nucleation mechanism predicts nucleation should occur outside the liquid. We hope to resolve such scales in future work, but the current equipment does not yet permit it.

[1] M. Baker, Science **276**, 1072 (1997).
[2] W. Cantrell and A. Heymsfield, Bull. Am. Meteorol. Soc. **86**, 795 (2005).
[3] L. J. Rothschild and R. L. Mancinelli, Nature **409**, 1092 (2001).
[4] B. Li and D.-W. Sun, J. Food Eng. **54**, 175 (2002).
[5] A. Gettelman, X. Liu, S. J. Ghan, H. Morrison, S. Park, A. Conley, S. A. Klein, J. Boyle, D. Mitchell, and J.-L. Li, J. Geophys. Res. **115**, D18216 (2010).
[6] R. P. Sear, Internat. Mat. Rev. **57**, 328 (2012).
[7] M. J. Kreder, J. Alvarenga, P. Kim, and J. Aizenberg, Nat. Rev. Mat. **1**, 15003 (2016).
[8] C. Hoose and O. Möhler, Atmos. Chem. Phys. **12**, 9817 (2012).
[9] D. A. Knopf and P. A. Alpert, Faraday Disc. **165**, 513 (2013).
[10] D. Lamb and J. Verlinde, *Physics and Chemistry of Clouds* (Cambridge University Press, Cambridge, 2011).
[11] N. E. Dorsey, Trans. Am. Philos. Soc. **38**, 247 (1948).
[12] H. Kanno, R. Speedy, and C. Angell, Science **189**, 880 (1975).
[13] E. B. Moore and V. Molinero, Nature **479**, 506 (2011).
[14] G. Bullock and V. Molinero, Faraday Discuss. **167**, 371 (2013).
[15] L. Ladino Moreno, O. Stetzer, and U. Lohmann, Atmos. Chem. Phys. **13**, 9745 (2013).
[16] W. A. Cooper, J. Atmos. Sci. **31**, 1832 (1974).
[17] N. Fukuta, J. Atmos. Sci. **32**, 1597 (1975).
[18] R. A. Shaw, A. J. Durant, and Y. Mi, J. Phys. Chem. B **109**, 9865 (2005).
[19] Y. Djikaev and E. Ruckenstein, J. Phys. Chem. A **112**, 11677 (2008).
[20] C. W. Gurganus, J. C. Charnawskas, A. B. Kostinski, and R. A. Shaw, Phys. Rev. Lett. **113**, 235701 (2014).
[21] J. Niehaus and W. Cantrell, J. Phys. Chem. Lett. **6**, 3490 (2015).
[22] R. D. Davis, S. Lance, J. A. Gordon, S. B. Ushijima, and M. A. Tolbert, Proc. Natl. Acad. Sci. U.S.A. **112**, 15815 (2015).
[23] C. Hoose, J. E. Kristjánsson, J.-P. Chen, and A. Hazra, J. Atmos. Sci. **67**, 2483 (2010).
[24] C. Gurganus, A. B. Kostinski, and R. A. Shaw, J. Phys. Chem. Lett. **2**, 1449 (2011).
[25] F. Yang, R. A. Shaw, C. W. Gurganus, S. K. Chong, and Y. K. Yap, Appl. Phys. Lett. **107**, 264101 (2015).
[26] C. Gurganus, A. B. Kostinski, and R. A. Shaw, J. Phys. Chem. C **117**, 6195 (2013).
[27] X. Noblin, A. Buguin, and F. Brochard-Wyart, Eur. Phys. J. E **14**, 395 (2004).
[28] X. Noblin, A. Buguin, and F. Brochard-Wyart, Phys. Rev. Lett. **94**, 166102 (2005).
[29] H. Tan, C. Diddens, P. Lv, J. Kuerten, X. Zhang, and D. Lohse, Proc. Nat. Acad. Sci. U.S.A. **113**, 8642 (2016).
[30] See Supplemental Material at http://link.aps.org/supplemental/10.1103/PhysRevE.97.023103 for (i) a pure water droplet on a silica glass substrate before and during oscillation (top view) for Movie S1; (ii) a water droplet containing a trace of pump oil on a silica glass substrate before and during oscillation (top view) for Movie S2; (iii) a water droplet with a trace of pump oil on a vertically-oscillating silica glass substrate, prior to freezing (top view) for Movie S3; (iv) pure water droplet on a vertically oscillating PDMS substrate, prior to freezing (top view) for Movie S4; (v) for Figures S1–S6; (vi) a pure water droplet on a silica glass substrate subjected to vertical oscillation (side view) for Movie S5; (vii) a water droplet containing a trace of mineral oil on a silica glass substrate before and after start of oscillation (top view) for Movie S6.
[31] P. de Gennes, D. Quéré, F. Brochard-Wyart, and A. Reisinger, *Capillarity and Wetting Phenomena: Drops, Bubbles, Pearls, Waves* (Springer, New York, 2004).
[32] K. N. Collier and S. D. Brooks, J. Phys. Chem. A **120**, 10169 (2016).
[33] L. Landau and E. Lifshitz, *Statistical Physics* (Butterworth-Heinemann, Oxford, 1980).
[34] A. Kostinski and W. Cantrell, J. Atmos. Sci. **65**, 2961 (2008).
[35] R. Hickling, Nature **206**, 915 (1965).
[36] J. Hunt and K. Jackson, Nature **211**, 1080 (1966).
[37] J. Hunt and K. Jackson, J. Appl. Phys. **37**, 254 (1966).
[38] K. A. Jackson, *Kinetic Processes: Crystal Growth, Diffusion, and Phase Transformations in Materials* (John Wiley & Sons, New York, 2006).
[39] M. Schremb, I. V. Roisman, and C. Tropea, Phys. Rev. E **95**, 022805 (2017).
[40] Z. Pan, A. Kiyama, Y. Tagawa, D. J. Daily, S. L. Thomson, R. Hurd, and T. T. Truscott, Proc. Natl. Acad. Sci. USA **114**, 8470 (2017).
[41] J. R. Espinosa, A. Zaragoza, P. Rosales-Pelaez, C. Navarro, C. Valeriani, C. Vega, and E. Sanz, Phys. Rev. Lett. **117**, 135702 (2016).
[42] T. Li, D. Donadio, and G. Galli, Nat. Commun. **4**, 1887 (2013).
[43] T. Němec, Chem. Phys. Lett. **583**, 64 (2013).
[44] M. Nosonovsky and B. Bhushan, Phys. Chem. Chem. Phys. **10**, 2137 (2008).
[45] I. Borzsák and P. T. Cummings, Fluid Phase Equilib. **150**, 141 (1998).
[46] F. Caupin, J. Non-Cryst. Solids **407**, 441 (2015).
[47] A. J. Page and R. P. Sear, Phys. Rev. Lett. **97**, 065701 (2006).
[48] A. Soare, R. Dijkink, M. R. Pascual, C. Sun, P. W. Cains, D. Lohse, A. I. Stankiewicz, and H. J. Kramer, Crystal Growth and Design **11**, 2311 (2011).
[49] A. Kiselev, F. Bachmann, P. Pedevilla, S. J. Cox, A. Michaelides, D. Gerthsen, and T. Leisner, Science **355**, 367 (2016).
[50] A. Alkezweeny, J. Appl. Meteorol. **8**, 994 (1969).
[51] R. D. Davis and M. A. Tolbert, Sci. Adv. **3**, e1700425 (2017).
[52] B. Wang, D. A. Knopf, S. China, B. W. Arey, T. H. Harder, M. K. Gilles, and A. Laskin, Phys. Chem. Chem. Phys. **18**, 29721 (2016).
[53] D. Lohse and X. Zhang, Rev. Mod. Phys. **87**, 981 (2015).